Anthropomorphic Grasp Synthesis Based on the Object Dynamic Properties

Vincenzo Lippiello

***Abstract*—The synthesis of optimal grasp configurations of heavy objects with anthropomorphic hands benefits from the explicit consideration of the object dynamic properties. A new solution for the fast synthesis of anthropomorphic grasps that ensures the reduction of gravitational and inertial effects during the execution of manipulation tasks as well as an equal distribution of the grasping forces among all fingers is proposed in this paper. The reduction of the computational complexity is achieved by considering only the regions of the object surface favoring the synthesis of minimal inertia grasps. Moreover, the hand and fingertip size, the hand kinematics, the object model uncertainty, and the surface curvature are all employed to further reduce the number of discrete grasping regions selected for the computation of the optimal grasp configurations with respect to a number of grasp quality indices. The effectiveness of the proposed method has been demonstrated with several case studies.**

***Index Terms*—Grasp synthesis, grasping, anthropomorphic hands.**

I. Introduction

The capability of a robotic hand to guarantee a firm grasp is an essential requirement for the manipulation of an object. The stability of a grasp configuration, as well as the disturbance resistance capability and the dexterity during a manipulation motion, are severely affected by the weight and inertia of heavy object. A large part of the available joint torques of the hand could be wasted due to inadequate grasp configurations [1], [2], thus limiting the manipulability. For this reason, an optimal grasp synthesis should explicitly take into account these factors.

An overview of techniques for 3D object grasp synthesis with multi-fingered robotic hands is proposed in [3] and with a focus on analytical and empirical approaches in [4]. A more general overview of grasping is presented in [5]. A method toward planning robot grasps across objects with similar parts is presented in [6]. In particular, the topological decomposition of objects proposed in this paper enables high-level semantic grasp planning. An algorithm for the on-line grasp planning of unknown objects with multi-fingered robotic hands is proposed in [7], [8]. In details, a visual object-surface reconstruction algorithm and a local grasp planner evolve in parallel generating a suboptimal grasp trajectory.

The research leading to these results has been supported by the RoDyMan project, funded by the European Community's Seventh Framework Programme (FP7/2007-2013) under ERC AdG-320992. The author is solely responsible for the content of this paper, which does not represent the opinion of the European Community, and the Community is not responsible for any use that might be made of the information contained therein.

V. Lippiello is with PRISMA Lab, Department of Electrical Engineering and Information Technology, University of Naples Federico II, via Claudio 21, 80125, Naples, Italy (email: vincenzo.lippiello@unina.it).

The off-line computation of a context-independent, i.e. where only the robot gripper and the target object are considered, and dense set of grasp configurations, instead of a small set of configurations regarded as optimal by using a given criterion, are proposed in [9]. The achieved set is then used on-line allowing the robot to quickly choose a suitable grasp for a given situation.

The combination of several grasp quality indices for the synthesis of optimal grasp configurations has been employed by a number of methods proposed in the literature. An overview of the most employed grasp quality indices is proposed in [10]. Several non-dimensional performance indices are proposed in [11], [12], where the problem of merging quality indices with different physical meaning is specifically addressed.

Combinations of different grasp quality indices are typically employed to achieve a global quality measure ranking all possible grasps either in a *parallel* or in a *serial* way. The parallel approach merges different quality indices into a global one. The algebraic (weighted) sum of a set of quality indices is considered in [13], where it has been assumed that all of them have to be either maximized or minimized. On the other hand, a significant grasp quality measure (or a proper combination) is employed with the serial approach to generate candidate grasp configurations. The best candidate is finally chosen by using a secondary quality measure (or a proper combination), resulting in a prioritized synthesis criterion [14].

The computational complexity of the optimal grasp search algorithms is an important aspect to take into account. In the case of polyhedral objects, being the most investigated ones, the evaluation of the force-closure regions can be cast into a linear programming problem [15], [16], which is computationally efficient, while the optimal grasp configuration can be chosen by solving a nonlinear programming problem [17]. In [18] a solution for grasp synthesis and fixture layout design in discrete domain has been presented. By solving a single linear program with an overall complexity of $O(N)$, given a number of candidate contact points on the object surface, this method allows the evaluation of a minimal subset from the candidate points so that they generate a grasp or a fixture with the form-closure property.

In [19] the effect of the number and type of engaged "postural synergies" have on the choice of grasping forces, and on the ultimate quality of the grasp, has been investigated. Numerical results have been presented showing the role played by different synergies in making a number of different grasps possible. Anthropomorphism has been exploited in [20], [21] for the development of a human-like grasping approach based on the synergic motions that can be observed in the human

hand. In [22], through the analysis of a quasi-static model, grasp structural properties related to contact force and object motion controllability have been defined. Motivated by the need for a means for robots operating in unstructured environments to robustly grasp and manipulate a wide range of objects using a multipurpose hand, in [23] an underactuated finger design and grasping method for precision grasping and manipulation of small objects has been demonstrated. Starting from these recent results, on one hand new compact grasp quality indices could be derived and employed for the grasp synthesis, and on the other hand the grasp of unknown objects can be achieved by employing complaint models, e.g. "soft synergies", or suitable mechanical designs to control the interaction forces and ensure both force closure and manipulability of the grasp.

In [24] the finger positioning error during the grasping and its consequence to the force-closure property are considered. In particular, the concept of Independent Contact Regions (ICRs) has been proposed providing robustness to the grasp, i.e. the force closure is guaranteed when finger contact occurs anywhere inside each of these regions, despite the exact contact position. A realistic modeling of the contact between the robotic fingers and an object has been used in [25] for the synthesis of multi-fingered grasps. A patch contact model has been adopted to locally approximate the contact between a rigid object and a deformable finger as a set of ICRs.

In this paper, the work presented in [26], [27] is specialized to the case of anthropomorphic robotic hands to quickly synthesize optimal n-fingered grasps for 3D objects with any shape ensuring the minimization of gravitational and inertial effects. The computational complexity is reduced by performing a suitable discretization of the object surface and a simultaneously selection of the pieces of surfaces suitable to generate optimal grasps. Differently from the existing approaches, this step is made under the lead of constraints derived from important grasp quality indices, that allow a strong reduction of the computational complexity. In detail, the presented method requires initially the evaluation of regions that can generate grasps with minimal gravitational and inertial effects. The achieved set of regions are further discretized on the basis of the local surface curvature, resulting in a set of groups of regions with a uniform curvature (e.g. planar regions, concave regions, convex regions, and angular regions). The fingertip size as well as the object model uncertainty are considered to further decompose the achieved regions. The search space of the optimization algorithm is hence reduced by applying linear constraints derived from the kinematics of the anthropomorphic hand and by taking into account the peculiarity of the thumb finger, which is the main opposite finger of the hand. Finally, a set of grasp quality indices is applied ranking the grasps according to a serial approach that takes into account the computational complexity of the chosen quality measures. The proposed method is particularly useful for the manipulation of heavy objects, compared to the hand capabilities, thanks to the choice of the inertial quality metrics. A number of objects with several shapes are presented to show the effectiveness of the proposed approach in terms of both computational time and quality of the grasp configuration with respect to a given anthropomorphic hand.

A MATLAB demo toolbox endowed with wizards to generate both suitable 3D MATLAB models from standard STL files and optimal grasps is provided[1].

II. Object surface discretization

The discretization of the object surface is crucial for the grasp synthesis because it severely affects the effectiveness, in terms of the final grasp quality, and the computational complexity. A rough discretization characterized by a low number of graspable regions decreases the computational complexity, but there is the risk that the best grasps could be cut off. In fact, a fine discretization results in a large number of regions that should endure the capability of the algorithm to find the best grasp but increases exponentially the computational time (see Section V-C), hence reducing the possibility to compute on-line the best grasp.

The proposed solution is based on the adoption of some grasp quality measures and hand properties to lead the object surface discretization and selection process [27]. The main idea consists into the selection and aggregation of those parts of the object surface capable to generate grasp configurations that are optimal for the dynamic object grasping and manipulation, i.e., optimal from an inertial point of view, and that are suitable to be reached by the hand fingertips.

This goal is achieved in three steps. First, the *minimal inertia regions* (MIRs) of the object surface, i.e. those parts of the object surface that can generate grasp configurations suitable from an inertial point of view, are found. Being this step computationally efficient, a high resolution of the object surface discretization can be used without affecting significantly the algorithm performances. Then, the MIR set is clustered into *uniform curvature regions* (UCRs). The result of this step is a very small number of connected regions that are characterized by similar geometrical and inertial properties. Finally, the UCR set is decomposed into a number of *grasp regions* (GRs) that are suitable to be reached by the fingertips of the employed hand and are dimensionally adequate. All the previous steps are explained in the following sections.

Notice that the 3D model of the object surface, e.g. a mesh representation, as well as the corresponding mass distribution, if the object density is not uniform, are assumed to be known.

A. Minimal inertia regions

The minimization of the grasp forces required for the compensation of the gravitational and inertial force is chosen as a main criterion for the MIR elements selection. This goal

[1] A MATLAB demo toolbox to test the proposed approach is available at the following address: http://wpage.unina.it/lippiell/docs/pubs/OGS_RAM2013_Matlab_Demo.zip. Wizards have been provided both for the construction of suitable MATLAB 3D models from standard STL files and for the optimal grasp synthesis. All the STL files of the employed 3D models are provided to recreate the figures included into the paper. Notice that this code is designed for a demonstration use only and it is not optimized as the one written in C++ employed for the performance tests of the paper. However, although some simplifications have been introduced for the demo purpose (e.g. the hand kinematic description and the accessibility test), the main optimization algorithm is analogous to the C++ version. We experienced that this code could be eight/ten times slower than the corresponding C++ version.

can be achieved by minimizing the distance between the object *center of gravity* (CoG) and the center of grip [13].

However, by adopting this criterion only the positions of the grasp points are taken into account, while the direction of the action lines of the contact forces are ignored. In fact, the "ideal" condition to compensate the gravity and inertial forces is achieved when the lines of action of the grasp forces have an isotropic angular distribution and are directed towards the object CoG. These criteria are known as *Focus Centering* and *Force Arrangement*, as quality indices for the grasp assessment, and *Real Focus Centering*, as a quality index for the configuration assessment [13], [28]. Without loss of generality, the case of hard fingers and point contact with friction is considered. Hence, when the *friction cone* (FC) of each grasp point contains the CoG of the object, then the corresponding center of grip remains close to the CoG. Under this favorable condition stable grasp configurations with respect to gravitational and inertial wrenches can be computed.

In view of the above considerations, the MIRs are defined as those portions of the object surface where the corresponding FC contains the CoG $\boldsymbol{c}_m$ for a given friction coefficient μ.

Let $\mathcal{S}$ be a 3D representation of the object surface, that can be extracted from an available CAD model or built with a visual system [7] or a tactile inspection [29], [30]. The finite MIR set is defined as the set of all the connected regions

$$\mathcal{R}_I = \{\mathcal{R}_{I1}, \ldots, \mathcal{R}_{Ii}\} \subseteq \mathcal{S} \tag{1}$$

such that

$$\boldsymbol{n}^{\mathrm{T}}(\boldsymbol{p})\boldsymbol{c}(\boldsymbol{p}) \leq \cos(\arctan(\mu)) \qquad \forall \boldsymbol{p} \in \mathcal{R}_I, \tag{2}$$

where $\boldsymbol{c}(\boldsymbol{p})$ is the *unit central vector*, here defined as the unit vector pointing from the contact point $\boldsymbol{p}$ to $\boldsymbol{c}_m$, and $\boldsymbol{n}(\boldsymbol{p})$ is the inward unit vector normal to the object surface at $\boldsymbol{p}$, as shown in Fig. 1.

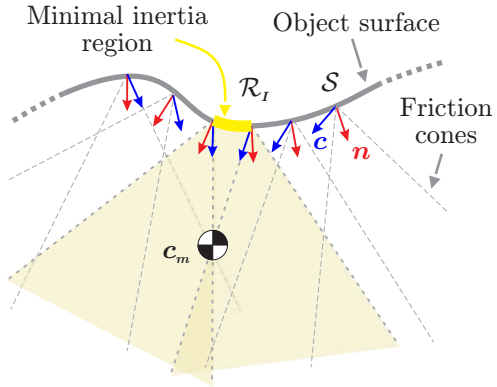

Fig. 1. Minimal inertia regions $\mathcal{R}_I$ (in yellow) for a portion of an object surface $\mathcal{S}$ (in gray).

According to the above considerations, the choice of the grasp points in $\mathcal{R}_I$ limits the synthesis of the best grasps to those capable of good gravitational and inertial effects compensation. Moreover, having selected only portions of the object surface, the computational time needed for the grasp synthesis will be reduced, too.

B. Uniform curvature regions

By further dividing each region of $\mathcal{R}_I$ into smaller connected subregions with uniform curvature, a new set of regions, namely uniform curvature regions (UCRs), is achieved

$$\mathcal{R}_C = \{\mathcal{R}_{C1}, \ldots, \mathcal{R}_{Cu}\} \subseteq \mathcal{R}_I. \tag{3}$$

The regions of $\mathcal{R}_I$ are partitioned into smaller connected subregions on the basis of similar values of the local curvature.

Let $k(\boldsymbol{p}) \in [-1, 1]$ be the curvature of the object surface at point $\boldsymbol{p}$ [27]. In this paper, five types of UCRs are considered: 1) planar region, for $|k| \leq k_p$; 2) convex region, for $k_p < k < k_a$; 3) convex corner region, for $k \geq k_a$; 4) concave region, for $-k_a < k < -k_p$; 5) concave corner region, for $k \leq -k_a$ (see Fig. 2). The thresholds k_p and k_a, with $0 < k_p < k_a < 1$, are employed for discriminating planar from convex, concave and corner regions, respectively.

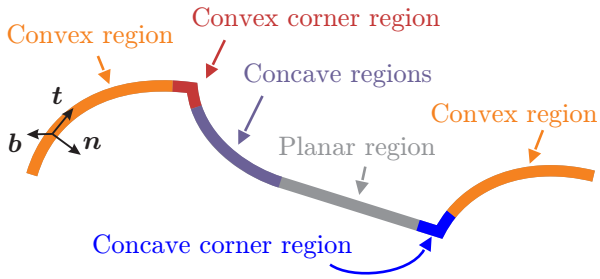

Fig. 2. Uniform curvature regions represented on a portion of an object surface.

A concave region produces a contact that is more stable than a planar and a convex one, as it was analytically demonstrated in [31]. Starting from this assumption, each class of region is ranked differently according to its capability to ensure stable contacts. This curvature ranking is employed during the grasp configuration synthesis step as a measure of the stability of the contact. Angular regions (regions with a high curvature) require specific considerations. As shown in [31], convex angular regions can produce unstable contacts, and thus they should be penalized during the grasp configuration selection. On the other hand, concave angular regions can produce stable contacts, however the real contact between the fingertip and the object surface is typically placed in an unpredictable point, also due to model inaccuracy. This condition could lead to uncertain grasps. For these reasons, all angular regions are strongly penalized during the grasp region ranking and they will be "de facto" discarded if other regions are available.

C. Grasp regions

The grasp regions (GRs) set is defined as the finite set of connected regions on which a stable and safe contact can be achieved. The elaboration of the GRs is executed by extracting a number of smaller regions from each region of $\mathcal{R}_C$, with a size suitable to accommodate a fingertip and uniformly distributed on it, hence

$$\mathcal{R}_G = \{\mathcal{R}_{G1}, \ldots, \mathcal{R}_{Gr}\} \subseteq \mathcal{R}_C. \tag{4}$$

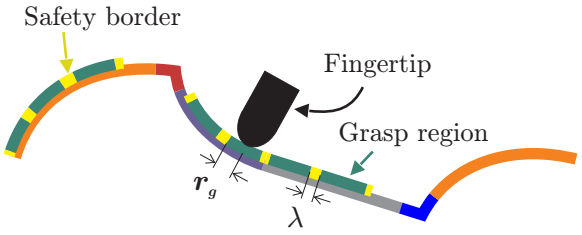

Fig. 3. Graphical representation of the grasp regions (green) and safety borders (yellow) represented on a portion of an object surface discretized on the basis of the minimal-inertia and uniform curvature criteria.

Grasp regions composed by points at a maximum distance $r_g > 0$ from a region central point are considered in this paper, where r_g is chosen equal to the tip radius.

Both the finger size and the accuracy of the CAD model are two of the most influencing factors for the GRs extraction process. By considering only these main factors, a uniform distribution of the GRs among $\mathcal{R}_C$ can be chosen as a selection criteria (see Fig. 3). A safety border with a radial dimension $\lambda > 0$ is added to each "circular" grasp region ensuring a safe fingertip contact also in the presence of model uncertainty. The tuning of λ depends directly on the model uncertainty, i.e. a good CAD model is given a smaller λ and viceversa. In any case, a safety border at least equal to the $5-10\%$ of r_g should be considered also to take into account the tips position errors.

To achieve a more effective decomposition of $\mathcal{R}_C$ a third parameter is considered, that is the aptitude to generate contact forces pointing toward the object CoG.

The following iterative selection algorithm is proposed for the grasp region selection process:

1) A region of $\mathcal{R}_C$ that has not yet been elaborated is set as "processing" region $\mathcal{R}_p$ and the process goes to step 2; if all the regions of $\mathcal{R}_C$ have already been elaborated the process ends.
2) If the shape and size of $\mathcal{R}_p$ is sufficient to locate a new GR the process continues with step 3, otherwise $\mathcal{R}_p$ is discarded and the process restart from step 1.
3) The point $\boldsymbol{p}_{nc}$ of $\mathcal{R}_p$ that corresponds to the minimum angle between the normal vector $\boldsymbol{n}$ and the central vector $\boldsymbol{c}$ is detected, and the minimum distance d_m between $\boldsymbol{p}_{nc}$ and the contour of $\mathcal{R}_p$ is computed. Then, if $d_m \geq r_g + \lambda$, a new grasp region centered at $\boldsymbol{p}_{nc}$ is added to $\mathcal{R}_G$ and removed from $\mathcal{R}_p$; otherwise, if $d_m < r_g + \lambda$, a new grasp region is selected as close as possible to $\boldsymbol{p}_{nc}$. The process goes back to step 2.

The final size of $\mathcal{R}_G$ depends on the area of $\mathcal{S}$ with respect to the fingertip size and, obviously, on the object shape. Instead, it does not depend significantly on the resolution of the available CAD model. Notice that increasing the safety border dimension λ decreases the number of grasp regions.

III. Anthropomorphic Grasp Configurations

The on-line feasibility of the grasp synthesis is an important achievement of the proposed approach. To reach this result, an initial discretization/selection of the object surface producing a finite set of GRs is applied, as described in the previous section. Even though the size of $\mathcal{R}_G$ is a small number for objects of size compatible with an anthropomorphic hand, the evaluation of all possible combinations up to 5 fingered grasps becomes quickly untractable for on-line applications. Moreover, most of the these combinatory grasps are ineffective and unfeasible, e.g. due to the hand kinematics and size.

In this paper we propose a new approach to reduce the grasps research space to those ones that can produce stable and inertial effective grasps. In particular, the peculiarity of the anatomic conformation of the anthropomorphic hand, which is endowed with a thumb finger opposing the other fingers in stable and powerful grasps, is fully considered. In fact, the GRs set is employed to locate the thumb fingertip for each of the considered grasp configurations. Thanks to the properties of the GRs set, the contact of the thumb in those regions allows the hand to provide a force with a line of action directed towards the CoG. Let $\boldsymbol{p}_c \in \mathcal{R}_G$ be the central point of a given GR. The opposite point $\boldsymbol{p}_o(\boldsymbol{p}_c, \boldsymbol{c}(\boldsymbol{p}_c))$ to $\boldsymbol{p}_c$ with respect to the CoG —the point corresponding to the intersection with the object surface of the half straight line starting from $\boldsymbol{p}_c$ and direct along $\boldsymbol{c}(\boldsymbol{p}_c)$— is considered as the main point leading the location of the other opposite fingers of the hand (in case of multiple intersections, the farther points are considered). The method proposed in [32] can be employed for the opposite point computation. With this approach, well described in the following sections, the number of grasp configurations that have to be evaluated during the grasp ranking test increases only linearly with the size of $\mathcal{R}_G$. In particular, the following policies will be used in reason of the desired number of fingers for the grasp synthesis.

A. Two-fingered grasps

In the two-fingered grasp case, for each region of $\mathcal{R}_G$, the contact point of the thumb finger is located in the center of the region and only the location of the opposite fingertip has to be determined. The point $\boldsymbol{p}_o$ is the starting candidate, as shown in Fig. 4. If a grasp region exists close to $\boldsymbol{p}_o$, the contact point is chosen in its center. More in general, $\boldsymbol{p}_o$ could be far from any region of $\mathcal{R}_G$. In this latter case, the achieved grasp configuration, i.e. the current grasp region, is discarded because it does not guarantee the force closure. On the other hand, for the case $\boldsymbol{p}_o \in \mathcal{R}_G$ several grasp feasibility tests are applied to the candidate grasp configuration.

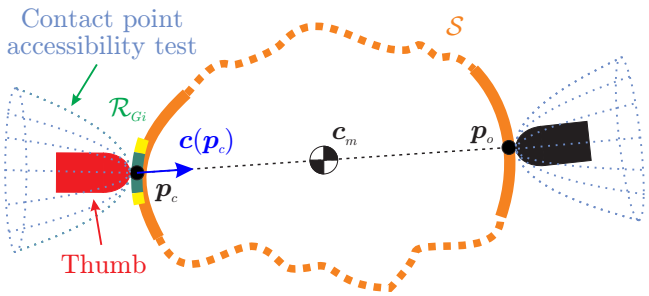

Fig. 4. Two-fingered grasp configuration.

First, the distance $d_{co} = \|\boldsymbol{p}_c - \boldsymbol{p}_o\|$ between the two fingers is compared to the maximum aperture for the available hand.

Then, the accessibility of each contact point is evaluated by verifying if a suitable free space is available in the proximity of the contact region. To achieve this goal the volume around the candidate contact point is sampled with a finite number of points (see Fig. 4); then, if all those test points are outside from the object the contact point under test is assumed reachable.

Finally, the existence of a hand pose (position and orientation) compatible with the current contact points candidates that avoid the contact of the palm with the object is verified. In particular, this test is performed by approximating the 2-fingered hand with a semi-elliptical shape sized in a conservative way with respect to the real hand size and the finger aperture (see Fig. 5). This semi-ellipse is first placed with the vertices in the contact point and is then progressively rotated around $\boldsymbol{c}(\boldsymbol{p}_c)$ of a small angles step. If at least one orientation exists that does not generate an intersection with the object surface, the grasp is accepted as a valid candidate for the final ranking step. The intersection is verified by sampling the semi-elliptical curve and by applying the method proposed in [32]. The rotational angles that correspond to feasible hand poses for the 2-fingered grasp candidate is a sub-result of this method.

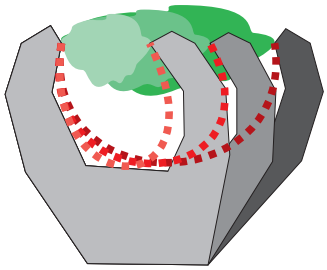

Fig. 5. Palm intersection test for different apertures of the hand.

B. Three-fingered grasps

The 3-fingered grasp configuration is achieved by locating the thumb on the current grasp region at point $\boldsymbol{p}_c$, as for the previous case. The contact points of the other two opposed fingers are computed starting from the point $\boldsymbol{p}_o$ as follows. First, we assume that the angle ϑ_F characterizes the opposed fingers aperture with respect to the thumb vertex (see Fig. 6). Without loss of generality, we assume that the angle ϑ_F between two consecutive opposed fingers is constant with the hand aperture and with the number of fingers. In a more general case, ϑ_F decreases with the hand aperture and the number of fingers. Then, a circular cone with apex at $\boldsymbol{p}_c$, aperture $\vartheta_F/2$, and $\boldsymbol{p}_o$ lying on the symmetry axis is employed to generate a set of contact point couples. In particular, the cone directrix is sampled with a fixed angular step. For each sampled point, the opposed point of the directrix with respect to cone base center is considered, so achieving a couple of half lines starting from $\boldsymbol{p}_c$ and intersecting $\mathcal{S}$ in a couple of candidate opposed contact points, namely $\boldsymbol{p}_{o1}$ and $\boldsymbol{p}_{o2}$, as shown in Fig. 6. Small local adjustment of the contact points can be applied in the case of proximity of grasp regions. Notice that the number of grasp configuration candidates so generated for each grasp region depends linearly on the number of samples kept on the directrix.

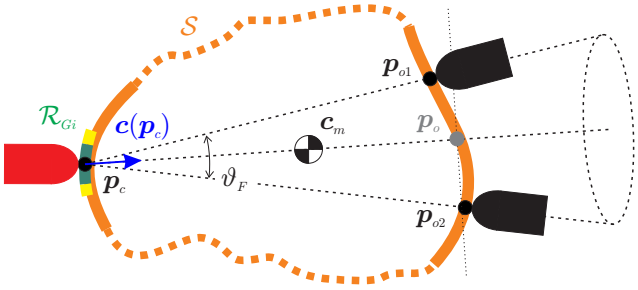

Fig. 6. Three-fingered grasp configuration.

The set of candidates is finally verified from the accessibility and feasibility point of view as in the previous case. First, the distances $d_{ci} = \|\boldsymbol{p}_c - \boldsymbol{p}_{oi}\|$, with $i = 1, 2$, are compared to the maximum aperture for the available hand. In addition, also the distance $d_{12} = \|\boldsymbol{p}_{o1} - \boldsymbol{p}_{o2}\|$ between the two opposed fingers is verified with respect to the hand kinematic limits. Then, the existence of a hand pose avoiding the contact of the palm with the object is tested in a similar way as for the 2-fingered case. In this case, two semi-elliptical test curves are considered, both starting from $\boldsymbol{p}_c$ and arriving at $\boldsymbol{p}_{o1}$ and $\boldsymbol{p}_{o2}$, respectively. Only the grasp configurations that overcome these tests are considered for the final ranking step. The force closure test as well as other computational complex tests are performed only on a limited number of best grasp configurations, as better described in the next section.

C. Four-fingered grasps

The four-fingered grasp configuration case is similar to the previous one. The main difference is that the cone aperture angle becomes ϑ_F and an additional contact point (middle finger) is fixed at $\boldsymbol{p}_o \equiv \boldsymbol{p}_{o2}$ (see Fig. 7). The accessibility and feasibility tests are performed in a similar way to the three-fingered case.

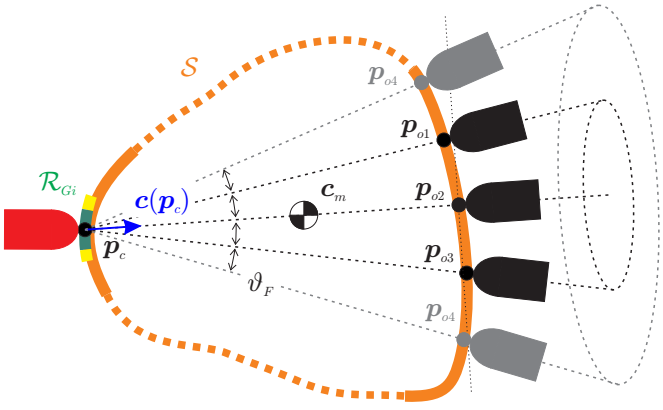

Fig. 7. Four/Five-fingered grasp configuration.

D. Five-fingered grasps

The selection of the fifth finger contact point candidate is made by adding a second cone with an aperture angle $2\vartheta_F a$, as shown in Fig. 7. Notice that in this case for each directrix

sample two different grasp configurations are achieved. In fact, the second cone allows finding two possible positions for the little finger. Also the accessibility and feasibility tests are performed similarly to previous cases.

IV. Grasp configurations ranking

Let $\mathcal{C}_n$, with $n = 2, \ldots, 5$, be the set of n-fingered grasp-configuration candidates computed with the previous procedure. Notice that if the object shape and size do not allow a suitable grasp with many fingers, e.g. with 5 fingers, the corresponding $\mathcal{C}_n$ are empty.

The optimal n-fingered grasp configuration is computed by ranking each grasp of $\mathcal{C}_n$ through a number of grasp measures in a hierarchical (i.e. serial) composition. The chosen quality measures have been split into two groups in a way to keep the computational complexity limited. The first group of indices is used in a hierarchical manner to rank $\mathcal{C}_n$. Then, at the end of the first ranking phase, the second group of indices, i.e. those ones with a higher computational complexity, is applied but starting from the best ranked configuration. All candidates which do not guarantee a suitable level for properties such as force closure, hand kinematic constraints, and manipulability are discarded until an optimal grasp is found. The priority composition method and a brief description of the adopted grasp quality indices are provided in the following sections.

A. Angular distribution and minimal inertia index

A uniform angular distribution of the grasp contact points increases the capability of the candidate grasp to stand up to external forces and disturbances [13], [33]. Moreover, if the contact force vectors point toward the object CoG, the gravitational and inertial effects are reduced too, thus achieving an isotropic dynamically-consistent grasp. To obtain this result, the composed quality index I_D proposed in [26] ranking the solid-angular distribution of the n-fingered grasp as well as the capability to reduce the gravitational and inertial effects is employed.

B. Extension index

The resistance capability of a grasp configuration with respect to external moments increases with the volume of the polyhedron having the grasp contact points as vertexes [34]. Therefore, an "extension" quality measure I_E that depends on the volume (i.e. on the area, in case of planar grasp) of the polyhedron can be considered.

C. Curvature index

The curvature quality index I_C is evaluated by summing an integer score assigned to the curvature of each contact region composing the current grasp configuration. Being the stability of the contact points conditioned by the curvature of the contact region, the following score is employed: 10 for concave angular region, 5 for convex angular region, 2 for convex region, 1 for planar region, 0 for concave region. As a result, grasp configurations with an index close to zero are characterized by a more stable contacts.

D. Grasp isotropy index

The grasp isotropy index I_G proposed in [10], [11] takes into account the closeness of the finger configurations to singular values. Notice that, only by avoiding the singular configurations, force control as well as precise position can be achieved during the object manipulation with a multi-fingered hand. Moreover, also the uniformity of the contact force contributions to the total wrench applied to the object depends on this quality measure. In fact, this index is close to 1 for isotropic grasp configurations, while it tends to zero for singular grasp configurations.

E. Force-closure test

The property of a grasps to resist any external force/moment applied to the object is known as force closure [35]. Being the computation of this property computationally expensive [36], the force-closure test is computed only for the best grasp configurations selected after the ranking procedure.

F. Hand and task kinematic indices

The overall quality of a grasp configuration also depends on the hand kinematic configuration and on the effectiveness with respect to an assigned task. Moreover, also some other aspects, such as joint limits and environmental constraints, should be considered [10]. Many quality indices have been proposed in the literature, most of which based on the analysis of the Jacobian matrix of the system composed by the hand and the object $\boldsymbol{G}^{\dagger \mathrm{T}} \boldsymbol{J}_h$, where $\boldsymbol{J}_h$ is the hand Jacobian, and $\boldsymbol{G}^{\dagger}$ is the generalized inverse of the grasp matrix. In particular, a weighted sum of a measure of the distance with respect to singular configurations and of the hand manipulability has been considered [26].

Notice that, in case of no redundant hand kinematics, the imposition of a grasp configuration fixes also the joint positions. Instead, in case of redundancy, it is known that infinite joint configurations correspond to the assigned grasp configuration, but it is always possible to choose the hand configuration maximizing the previous manipulability measure.

G. Grasp ranking

The grasp ranking is performed by computing the angular distribution and minimal inertia index, the extension index, and the curvature index for all the feasible grasp configurations in the sets $\mathcal{C}_n$, with $n = 2, \ldots, 5$. The dynamically-consistent approach adopted for the grasp region computation typically ensures a small value for the size of $\mathcal{C}_n$.

First, the sets of possible n-fingered grasps is inserted into the initial grasp ranking list $\mathcal{L} = \mathcal{C}_2 \cup \cdots \cup \mathcal{C}_5$, and the following three-level sort algorithm is executed:

1) *First sort level*: all grasp configurations present in $\mathcal{L}$ with a quality index I_D close to the current one (e.g. differing less than 5%) are selected, resulting in an ordered sublist $\mathcal{L}_D \subseteq \mathcal{L}$, for the next sort level; if none is found, the current configuration is sorted into $\mathcal{L}$ using I_D as ordering criterion and the elaboration of the current grasp candidate ends.

Fig. 8. From the top: the CAD models of the objects employed in the 3D case studies together with the corresponding minimal inertia regions (yellow), the uniform curvature regions (planar regions in gray, concave regions in violet, convex regions in orange, concave corner regions in blue, and convex corner regions in red), and the grasp regions (discs with the fingertips size and the same color convention adopted for the uniform curvature regions). The black sphere indicates the object center of gravity.

2) *Second sort level*: all grasp configurations of $\mathcal{L}_D$ with an index I_E close to the current one (e.g. differing less that 10%) are selected for the next sort level, resulting in an ordered sublist $\mathcal{L}_E \subseteq \mathcal{L}_D$; if none is found, the candidate grasp configuration is positioned into $\mathcal{L}_D$ using I_E as ordering criterion and the elaboration of the current grasp candidate ends.
3) *Third sort level*: the current configuration is inserted into $\mathcal{L}_E$ using I_C as ordering criterion.

At the end of the previous sort process, $\mathcal{L}$ contains an ordered list of the optimal grasp configurations that have been ranked using I_D as first-level ordering criteria, I_E as second-level ordering criteria, and I_C as third-level ordering criteria. In fact, the proposed multi-level sort criteria ensures that grasps with similar value of I_D turn out to be sorted with respect to the index I_E, while all the configurations with close values of I_E turn out to be sorted by using the index I_C.

After the ranking step, starting from the best ranked grasp configuration, the computationally expensive measures/tests are computed only until one (or more, if required by the application) grasp overcomes all the acceptance threashold/test. First of all, the force closure is evaluated, i.e. if the current grasp configuration is not force closure it is discarded and the next grasp of $\mathcal{L}$ is considered, otherwise the grasp isotropy index I_G is computed and compared to a suitable acceptability threshold. If the candidate best grasp does not overcome this threshold, the next grasp configuration of $\mathcal{L}$ is considered, otherwise the hand and task kinematic indices are computed to accept or discard the current best grasp. A grasp configuration exceeding all the previous tests is ranked as the best feasible grasp and the process ends.

V. Case studies

The proposed anthropomorphic-hand grasp synthesis algorithm has been tested on a number of 3D everyday objects evaluating the performance in terms of computational time and effectiveness of the candidate best grasp. Five different CAD models of a water glass, a wine glass, a mug, a shaped bottle, and a monster toy are considered to demonstrate the feasibility and the effectiveness of the proposed approach in several conditions depending on the CAD model resolution and on the employed number of fingers.

An anthropomorphic 5-fingered hand with a human like size has been employed for the hand kinematic grasp quality index as well as for the kinematic constraints test. The maximum grasp extension between the thumb and the other fingers has been limited to 12 cm in the feasibility tests. The adopted friction coefficient for all the employed objects is $\mu = 0.4$.

Triangle meshes with five different resolutions for each object have been used, i.e. from 1000 to 5000 faces. This range of values is suitable for the evaluation of the computational performance of the proposed method.

A. Grasp regions evaluation

The CAD models of the employed object (water glass, wine glass, mug, shaped bottle, and monster toy) together with the corresponding minimal inertia regions, the uniform curvature regions, and the grasp regions are shown in Fig. 8. The water glass is 9 cm high, the wine glass is 15 cm high, the bottle is 20 cm high, and the mug and the monster toy are 10 cm high.

The number of minimal inertial regions, of the uniform curvature regions, and of the grasp regions extracted from the CAD models of the considered objects are shown in Fig. 9, where five triangle mesh resolutions have been adopted: 1000, 2000, 3000, 4000, and 5000 faces, respectively. Notice how the size of $\mathcal{R}_I$ increases almost linearly with the object resolution [see Fig. 9(a)], as it was reasonably expected.

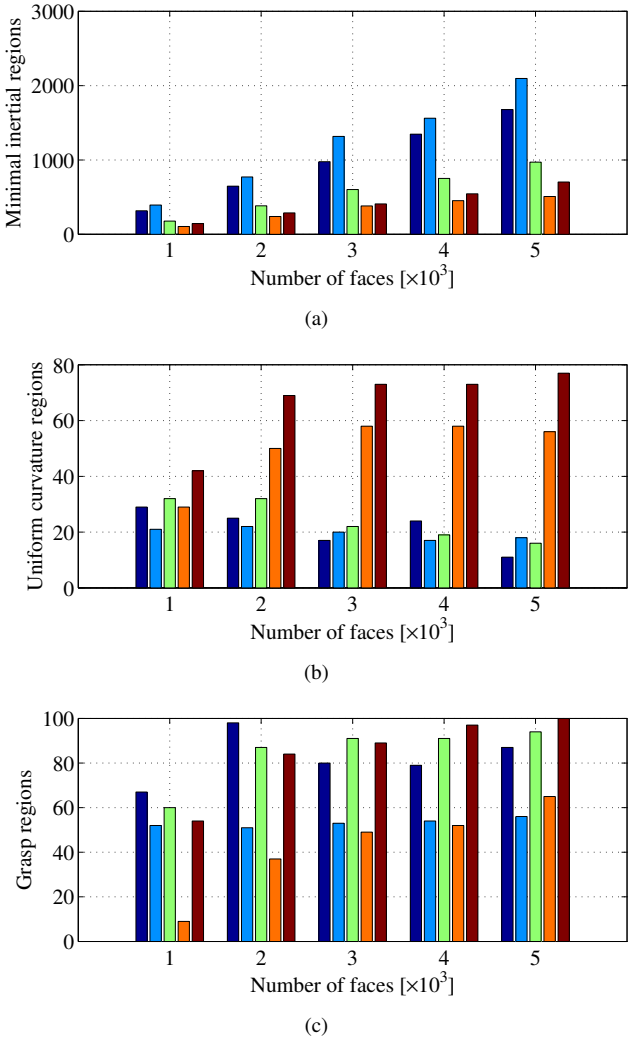

Fig. 9. Number of the minimal inertial regions (a), of the uniform curvature regions (b), and of the grasp regions (c) extracted from the CAD models of the water glass (dark blue), of the wine glass (light blue), of the mug (green), of the shaped bottle (red), and of the monster toy (brown) with different triangle mesh resolution.

Conversely, the size of $\mathcal{R}_C$ and of $\mathcal{R}_G$ increases with a sub-linear rate that depends on the object shape as shown in Figs. 9(b) and 9(c). However, this behavior is expected because the sizes of $\mathcal{R}_C$ and $\mathcal{R}_G$ have to become constant when the resolution increases being fixed the fingertip size.

B. Grasp synthesis

Figure 10 shows the best-ranked grasp configurations for the objects of Fig. 8 for the cases of $n = 2, \ldots, 5$ fingers. It

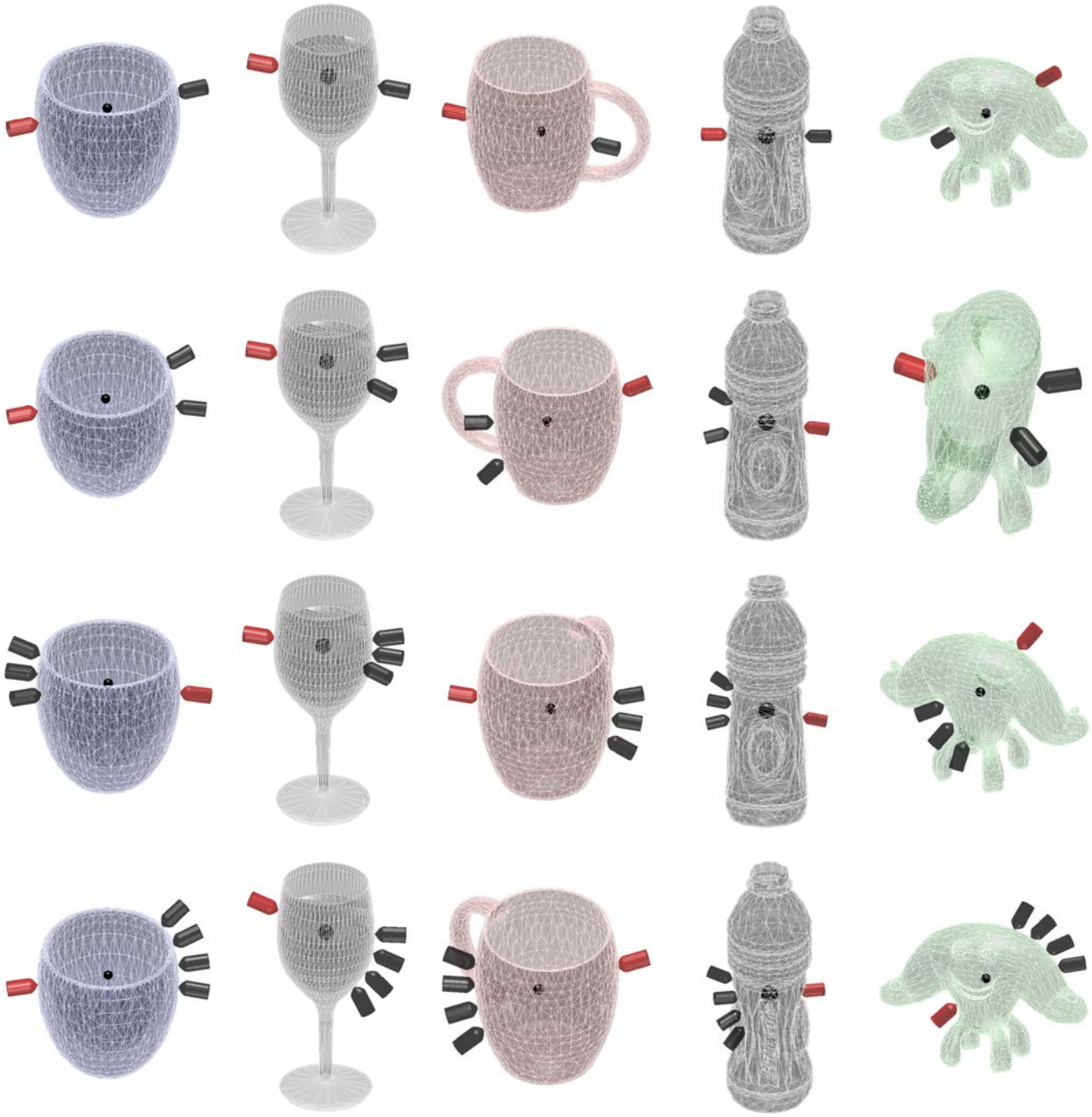

Fig. 10. Best-ranked grasps for the objects of Fig. 8 with $n = 2, \ldots, 5$ fingers (from the top to the bottom). The black sphere indicates the object CoG.

is worth noticing how, depending on the dimension and shape of the object, the best grasp candidates for each object by changing the number of employed fingers are very similar. This result confirms the numerical stability of the proposed algorithm. On the other hand, for very irregular objects, e.g. the monster toy on the right side of Fig. 10, the best grasp configurations change more with n due to the feasibility constraint, which depends on the possibility to touch the object with more fingers respecting the kinematic constraints.

The minimization of the gravitational effects has been tested by considering the case of a half-filled bottle, i.e. by changing the position of the center of gravity of the bottle with respect to the case shown previously. Figure 11 shows the corresponding best-ranked grasp candidates for $n = 2, \ldots, 5$ fingers. In all cases, the off-centering of the line of action of the applied fingertips forces is negligible, hence the compensation of gravitational effects is maximized.

C. Computational complexity

The computational complexity of the proposed method has been evaluated by measuring the computational time needed for the grasp synthesis of the best grasp candidate for the

Fig. 11. Best-ranked grasp configurations for the half-filled shaped bottle, i.e. when an offset is applied to the center of gravity.

objects of Fig. 8 with different triangle-mesh resolutions. The following test have been carried out on an Intel Pentium processor at 2.8 Ghz with C++ programming.

Figure 12 shows the computation time employed for the elaboration of the minimal inertial regions, on the uniform curvature regions, and of the grasp regions. As it was expected, an almost linear and increasing trend with respect to the object model resolution is clearly evidenced for this step. Notice that the absolute value of the time required for the computation of the grasp regions both for the shaped bottle (Fig. 12(d)) and for the monster toy (Fig. 12(e)) are about one order of magnitude less than for the other objects. The reason is because the corresponding uniform curvature regions, while being greater in number, are smaller in size due to the irregularity of the object shapes. Hence, in many cases there is not enough area for the fingertip and the region was discarded without participating to the (recursive and computationally expensive) decomposition process, that divides the each uniform curvature region into a number of grasp regions. However, for all the considered cases the needed computational time are reasonably low and compatible with an on-line application.

Figure 13 shows the overall computation times required for the grasp synthesis with respect to the number of employed fingers. For all the considered objects the computation time increases with respect to the number of fingers with a sub-linear rate. For the same cases, i.e. for the first three objects, the trend becomes descendent for $n = 5$. The reason of this behavior is the progressive reduction of the number of available contact regions suitable to allow the allocation of 5 fingertips under the minimization of the inertial effects and kinematic constraints. A further reason is that many of the best-ranked grasp regions for $n = 3, 4$ turn out to be inadequate after the feasibility tests (mainly due to the whole-hand reachability test, that fails for size and shape of the object) that are sequentially applied until a suitable grasp configuration is found. This last behavior represents also the most significant drawback of the proposed method, i.e. when several best-ranked grasp candidates are discarded before a suitable grasp is found. Being this test time consuming for the 3D case, then the total computation time increases. However, also in these worst cases the required computational time makes the proposed technique useful for on-line applications.

VI. Conclusion

The problem of evaluating grasp configurations which reduce the inertial and gravitational effects of an object on a robotic hand has been addressed in this paper. A new solution for fast synthesis of anthropomorphic multi-fingered grasp configurations has been proposed. Several 3D case studies have been presented showing the effectiveness of the proposed approach.

References

[1] V. Lippiello, B. Siciliano, and L. Villani, "A grasping force optimization algorithm for multiarm robots with multifingered hands," *IEEE Transactions on Robotics*, vol. 29, no. 1, pp. 55–67, 2013.

[2] V. Lippiello, B. Siciliano, and L. Villani, "A grasping force optimization algorithm for dexterous robotic hands," in *IEEE International Conference on Robotics and Automation*, pp. 4170–4175, 2012.

[3] A. Sahbani, S. El-Khoury, and P. Bidaud, "An overview of 3D object grasp synthesis algorithms," *Robotics and Autonomous Systems*, vol. 60, no. 3, pp. 326–336, 2012.

[4] D. Prattichizzo and J. C. Trinkle, "Grasping," in *Springer Handbook of Robotics* (B. Siciliano and O. Khatib, eds.), ch. 28, pp. 671–700, Springer Berlin Heidelberg, 2008.

[5] A. Bicchi and V. Kumar, "Robotic grasping and contact: A review," in *IEEE International Conference on Robotics and Automation*, vol. 1, pp. 348–353, 2000.

[6] J. Aleotti and S. Caselli, "A 3D shape segmentation approach for robot grasping by parts," *Robotics and Autonomous Systems*, vol. 60, no. 3, pp. 358–366, 2012.

[7] V. Lippiello, F. Ruggiero, B. Siciliano, and L. Villani, "Visual grasp planning for unknown objects using a multifingered robotic hand," *IEEE/ASME Transactions on Mechatronics*, vol. 18, no. 3, pp. 1050–1059, 2013.

[8] V. Lippiello, F. Ruggiero, B. Siciliano, and L. Villani, "Preshaped visual grasp of unknown objects with a multi-fingered hand," in *IEEE/RSJ International Conference on Intelligent Robots and Systems*, pp. 5894–5899, 2010.

[9] J.-P. Saut and D. Sidobre, "Efficient models for grasp planning with a multi-fingered hand," *Robotics and Autonomous Systems*, vol. 60, no. 3, pp. 347–357, 2012.

[10] R. Suárez, M. Roa, and J. Cornella, "Grasp quality measures," tech. rep., Technical University of Catalonia, 2006.

[11] B.-H. Kim, S.-R. Oh, B.-J. Yi, and I. H. Suh, "Optimal grasping based on non-dimensionalized performance indices," in *IEEE/RSJ International Conference on Intelligent Robots and Systems*, vol. 2, pp. 949–956, 2001.

[12] B.-H. Kim, B.-J. Yi, S.-R. Oh, and I. H. Suh, "Non-dimensionalized performance indices based optimal grasping for multi-fingered hands," *Mechatronics*, vol. 14, no. 3, pp. 255–280, 2004.

[13] E. Chinellato, A. Morales, R. Fisher, and A. del Pobil, "Visual quality measures for characterizing planar robot grasps," *IEEE Transactions on Systems, Man, and Cybernetics, Part C: Applications and Reviews*, vol. 35, no. 1, pp. 30–41, 2005.

[14] R. Hester, M. Cetin, C. Kapoor, and D. Tesar, "A criteria-based approach to grasp synthesis," in *IEEE International Conference on Robotics and Automation*, vol. 2, pp. 1255–1260, 1999.

[15] J. Ponce and B. Faverjon, "On computing three-finger force-closure grasps of polygonal objects," *IEEE Transactions on Robotics and Automation*, vol. 11, no. 6, pp. 868–881, 1995.

[16] C.-P. Tung and A. Kak, "Fast construction of force-closure grasps," *IEEE Transactions on Robotics and Automation*, vol. 12, no. 4, pp. 615–626, 1996.

[17] D. Ding, Y.-H. Lee, and S. Wang, "Computation of 3-D form-closure grasps," *IEEE Transactions on Robotics and Automation*, vol. 17, no. 4, pp. 515–522, 2001.

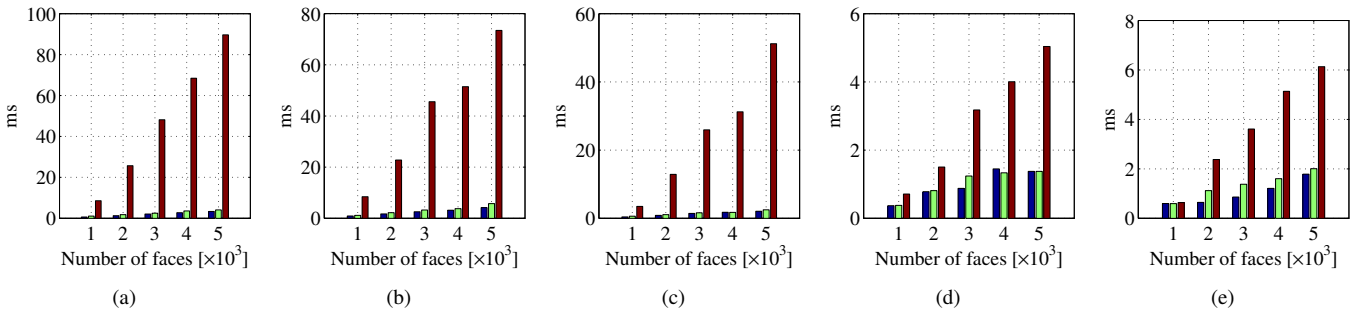

Fig. 12. Computation times needed for the selection of the minimal inertial regions (blue), of the uniform curvature regions (green), and of the grasp regions (red) from the CAD models of the water glass (a), of the wine glass (b), of the mug (c), of the shaped bottle (d), and of the monster toy (e) for a number of triangle mesh resolutions.

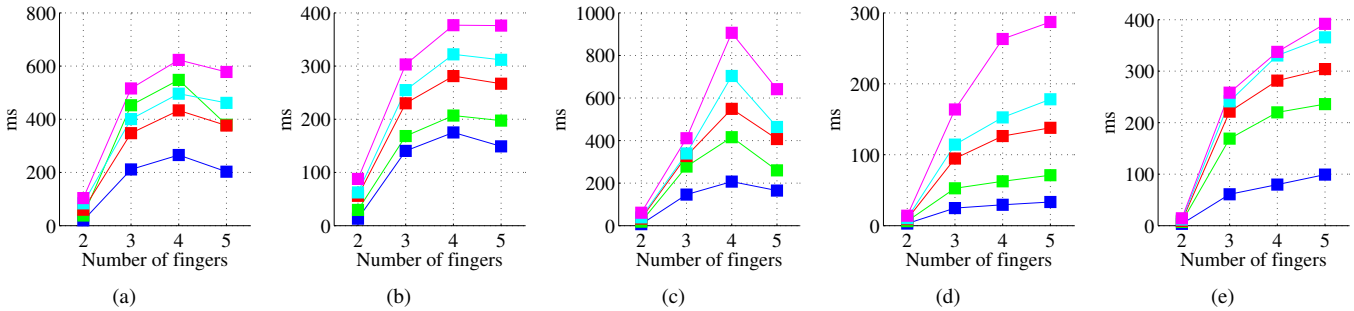

Fig. 13. Total computation times required for the evaluation of the best grasp candidates with a number of fingers $n = 2, \ldots, 5$ and for different CAD model resolutions (1000 faces in blue, 2000 faces in green, 3000 faces in red, 4000 faces in magenta, and 5000 faces in cyan). Five different objects are considered: a) water glass, b) wine glass, c) mug, d) shaped bottle, and e) monster toy.

[18] X. Zhu and H. Ding, "An efficient algorithm for grasp synthesis and fixture layout design in discrete domain," *IEEE Transactions on Robotics*, vol. 23, no. 1, pp. 157–163, 2007.

[19] M. Gabiccini, A. Bicchi, D. Prattichizzo, and M. Malvezzi, "On the role of hand synergies in the optimal choice of grasping forces," *Autonomous Robots*, vol. 31, no. 2-3, pp. 235–252, 2011.

[20] L. Villani, F. Ficuciello, V. Lippiello, G. Palli, F. Ruggiero, and B. Siciliano, "Grasping and control of multi-fingered hands," *Advanced Bimanual Manipulation*, vol. STARSpringer Tracts in Advanced Robotics, no. 80, pp. 219–266, 2012.

[21] F. Ficuciello, G. Palli, C. Melchiorri, and B. Siciliano, "Postural synergies of the {UB} hand {IV} for human-like grasping," *Robotics and Autonomous Systems*, vol. 62, no. 4, pp. 515 – 527, 2014.

[22] D. Prattichizzo, M. Malvezzi, M. Gabiccini, and A. Bicchi, "On motion and force controllability of precision grasps with hands actuated by soft synergies," *IEEE Transactions on Robotics*, 2013.

[23] L. Odhner, R. Ma, and A. Dollar, "Open-loop precision grasping with underactuated hands inspired by a human manipulation strategy," *IEEE Transactions on Automation Science and Engineering*, 2013.

[24] M. Roa and R. Suarez, "Computation of independent contact regions for grasping 3-D objects," *IEEE Transactions on Robotics*, vol. 25, no. 4, pp. 839–850, 2009.

[25] K. Charusta, R. Krug, D. Dimitrov, and B. Iliev, "Independent contact regions based on a patch contact model," in *IEEE International Conference on Robotics and Automation*, pp. 4162–4169, 2012.

[26] V. Lippiello, B. Siciliano, and L. Villani, "Fast multi-fingered grasp synthesis based on object dynamic properties," in *IEEE/ASME International Conference on Advanced Intelligent Mechatronics*, pp. 1134–1139, 2010.

[27] V. Lippiello, B. Siciliano, and L. Villani, "Multi-fingered grasp synthesis based on the object dynamic properties," *Robotics and Autonomous Systems*, vol. 61, no. 6, pp. 626–636, 2013.

[28] E. Chinellato, R. Fisher, A. Morales, and A. del Pobil, "Ranking planar grasp configurations for a three-finger hand," in *IEEE International Conference on Robotics and Automation*, vol. 1, pp. 1133–1138, 2003.

[29] V. Lippiello, B. Siciliano, and L. Villani, "Robot interaction control using force and vision," in *IEEE/RSJ International Conference on Intelligent Robots and Systems*, pp. 1470–1475, 2006.

[30] V. Lippiello, B. Siciliano, and L. Villani, "Interaction control of robot manipulators using force and vision," *International Journal of Optomechatronics*, vol. 2, no. 3, pp. 257–274, 2008.

[31] D. Montana, "The condition for contact grasp stability," in *IEEE International Conference on Robotics and Automation*, pp. 412–417, 1991.

[32] T. Mller and B. Trumbore, "Fast, minimum storage ray-triangle intersection," *Journal of Graphics Tools*, vol. 2, no. 1, pp. 21–28, 1997.

[33] B. Mirtich and J. Canny, "Easily computable optimum grasps in 2-D and 3-D," in *IEEE International Conference on Robotics and Automation*, pp. 739–747, 1994.

[34] C.-H. Xiong, Y.-F. Li, H. Ding, and Y.-L. Xiong, "On the dynamic stability of grasping," *The International Journal of Robotics Research*, vol. 18, no. 9, pp. 951–958, 1999.

[35] R. M. Murray, S. S. Sastry, and L. Zexiang, *A Mathematical Introduction to Robotic Manipulation*. Boca Raton, FL, USA: CRC Press, Inc., 1st ed., 1994.

[36] S. El-Khoury and A. Sahbani, "On computing robust n-finger force-closure grasps of 3D objects," in *IEEE International Conference on Robotics and Automation*, pp. 2480–2486, 2009.

Vincenzo Lippiello was born in Naples, Italy, on June 19, 1975. He received his Laurea degree in electronic engineering and the Research Doctorate degree in information engineering from the University of Naples, Naples, Italy, in 2000 and 2004, respectively. He is an Assistant Professor of Automatic Control in the Department of Electrical Engineering and Information Technology, University of Naples. His research interests include visual servoing of robot manipulators, hybrid visual/force control, adaptive control, grasping and manipulation, aerial robotics, robotic ball catching, and visual object tracking and reconstruction. He has published more than 90 journal and conference papers and book chapters. He is member of the IFAC Technical Committee on Robotics.